Article

Nonlinear Radiative Nanofluidic Hydrothermal Unsteady Bidirectional Transport with Thermal/Mass Convection Aspects

Muhammad Faisal [1], Kanayo Kenneth Asogwa [2], Nazek Alessa [3,*] and Karuppusamy Loganathan [4,*]

1 Department of Mathematics, Azad Jammu and Kashmir University, Muzaffarabad 13100, Pakistan
2 Department of Mathematics, Nigeria Maritime University, Okerenkoko 332105, Delta, Nigeria
3 Department of Mathematical Sciences, College of Sciences, Princess Nourah Bint Abdulrahman University, P.O. Box 84428, Riyadh 11671, Saudi Arabia
4 Department of Mathematics and Statistics, Manipal University Jaipur, Jaipur 303007, Rajasthan, India
* Correspondence: nazekaa@yahoo.com (N.A.); loganathankaruppusamy304@gmail.com (K.L.)

Abstract: The collective effect of thermal and mass convection along with the significance of thermal radiation, heat source/sink, and magneto-nanofluid are considered. A bi-directional stretching device is used to generate the symmetry of the flowing structure. Nonlinear behavior of thermal radiation is considered here. The magnetic field is considered non-uniform and vertically upward. Significances of pedesis motion and Ludwig–Soret are also revealed in an innovative way with heat source/sink effects. The concept of symmetry is used to transmute the transport equations from PDE type to nonlinear ODE type. We solved the transformed setup numerically by adopting Keller-box method criteria with the targeted accuracy rate. Graphical interpretations are explored with code verification. It is important to conclude that friction coefficients decline for incremental values of stretching parameter ($0.1 \leq \alpha \leq 0.9$), magnetic field ($0.3 \leq M \leq 0.9$), and unsteady parameter ($0.2 \leq \Lambda \leq 0.9$) along with the bidirectional velocity components, and the rate of heat transmission rises with temperature ratio ($1.3 \leq \Gamma \leq 1.7$) and temperature Biot number ($0.3 \leq Bi_T \leq 0.9$) amplification. Moreso, the rate of mass transfer is enhanced with growing values of pedesis motion ($0.2 \leq N_b \leq 0.6$), unsteady parameter and concentration Biot number ($0.3 \leq Bi_C \leq 0.9$) with opposite effect when the Ludwig–Soret parameter ($0.3 \leq N_t \leq 0.6$) is boosted.

Keywords: thermal/mass convection; unsteady flow; bidirectional stretching; nonlinear thermal radiation; heat source/sink; Keller-box method

1. Introduction

Fluid mechanics as an application point of view is a vast area of research in industrial and engineering sectors. It is difficult to neglect the laws of fluid dynamics in daily life activities, such as production of polymers, biomedicine manufactures, ventilation, pipelines system, plastic industries, oil refiners, aerospace, thermal trades, oxygen plants, hydro power projects, etc. Nonlinear thermal radiation energy at the surface of any plane structure in fluid mechanics is of tremendous importance, such as could be found in hydroelectric dams, production engineering, wind energy, and also medical sciences. Nonlinear thermal radiation, like electromagnetic fields, is transmitted in all directions from a radiating surface. Nonlinear thermal radiation energy is the process by which heat is transported via space by convection or conduction. Various engineering processes occur due to high temperature, which propelled the research study of Seddeek et al. [1] to address the implication of thermal radiation on unsteady MHD fluid flow. Mushtaq et al. [2] examined the radiation impact in 2D stagnation point flow of a nanofluid owing to solar energy. They revealed that wall temperature gradient is a rising function of the radiation parameter. Moreso, the increased mobility of nanoparticles in the base fluids culminates in the greater conversion of solar radiations in the fluids. Ramzan et al. [3] researched the flow of a hybrid nanofluid across a curved stretching surface using nonlinear thermal radiation. They concluded that

when the radiation and curvature characteristics were boosted, the Nusselt number reduced. Mahanthesh et al. [4] analyzed the heat transport phenomena under effect of bioconvection in order to optimize heat transfer attributes. They established that, in comparison to the thermophoresis impact, the heat transport rate is significantly sensitive to nonlinear thermal radiation coefficients. Using the RKF45 method with a shooting procedure, Rana et al. [5] studied the impacts of thermal radiation on a stretching/shrinking sheet in a slip flow of a nanofluid. It was revealed that thermal radiation increases temperature and nanoparticle volume fraction. Bhatti et al. [6] investigated entropy generation using nonlinear thermal radiation and chemical reaction interactions on Magnetohydrodynamic Williamson nanofluids. Recently, Adnan et al. [7] examined the behavior of nanofluids in a specific context of Cu-kerosene oil and Cu-water consisting of two Riga plates using unique effects of thermal radiation and surface convection. They discovered that when thermal radiations and surface convection are induced, the temperature of Cu-kerosene oil and Cu-water considerably increases, and the local Nusselt number increases as a result of the altering thermal radiation. Mustafa et al. [8] investigated the dynamics of nanofluid through a natural convective surface via a vertical medium in the presence of nonlinear radiative heat flux. They discovered that as the radiation parameter is increased, the temperature rise and heat transfer from the plate diminishes. Muhammad et al. [9] investigated Carreau nanofluid bioconvection transmission using a magnetic dipole and nonlinear thermal radiation. Khan et al. [10] investigated the effects of nonlinear radiation on the MHD flow of a nanofluid across a nonlinearly elongating wedge.

At the present time, researchers are analyzing nanofluid flows caused by a bidirectionally stretchable surface owing to its remarkable applications in paper production, particle growing, fibre and glass, cooling of fabrics, evaporative cooling, fibrous insulating layers, groundwater sources, fractional distillation, among others. By definition, this novel phenomenon known as bidirectional stretching is actually stretching proceeds in the x and y axes. Ramzan and Yousaf [11] investigated the three-dimensional drift of nanofluid moving on a bidirectional stretchy surface. Hayat et al. [12] investigated the bidirectional flow of a radiative viscoelastic nanomaterial driven by an expanding sheet in the presence of energy stored. Javed et al. [13] investigated the effect of viscous dissipation and Joule heating on Prandtl nanofluid flow induced by an unsteady bidirectionally moving surface. Ahmad et al. [14] investigated the effect of ceria and zinc-oxide nanocomposites on the time dependent 3D transmission of a water-driven hybrid nanofluid over a bidirectional stretched sheet coupled with a heat source/sink. To improve energy systems' effectiveness, Khan et al. [15] investigated the double stratification three-dimensional flow of Burgers nanofluid, including microorganisms, across a bidirectional stretched surface. Faisal et al. [16] surveyed the bidirectional flow of Casson nanomaterial powered by an unsteady moving surface in the boundary layer region using a suitable Keller-box method, taking into account the implications of prescribed surface temperature. Gupta and Gupta [17] noticed a stream of an Oldroyd-B typed nanocomposite in a three-dimensional framework on a bidirectional extensible surface. Bag and Kundu [18] analyzed thermal radiation nanofluidic transfer over a bidirectional stretched sheet with diverse convective regimes and a heat source/sink. Ahmad et al. [19] evaluated thermal stratification, chemical reaction, and solutal stratification of time dependent three-dimensional bidirectional stretching flow of an Oldroyd-B nanofluid. Munir et al. [20] evaluated the flow and heat transmission properties of a 3D Sisko fluid controlled by a bidirectional stretching sheet. Bilal et al. [21] addressed the MHD 3D boundary layer flow of Williamson fluid regulated by a bidirectional stretched surface using the Runge–Kutta algorithm in conjunction with the shooting method. Other relevant research work could be cited in [22–25].

The Ludwig–Soret effect and pedesis motion are critical for comprehending the phenomena of heat and mass movement. The Ludwig–Soret effect or thermophoresis is a physical phenomenon that occurs in combination of moving particles when the varying particle kinds respond differently to the force of a temperature gradient. The terminology thermophoresis is most frequently used to refer to aerosol mixtures. Typically, the phrase

"Soret Effect" refers to liquid mixes, which behave differently and through fewer known mechanisms than gaseous mixtures. On the other hand, pedesis or Brownian motion is the random motion of suspended particles in a fluid. The motion is caused by collisions between fast-moving molecules or atoms and the particles. The Ludwig–Soret effect and pedesis motion is critical in practically all industrial processes. It is utilized in industrial operations to conserve energy and shorten processing times. Afify [26] scrutinized the Brownian movement and thermodiffusion impact on Casson nanofluid flow with convective boundaries. Comparing non-Newtonian fluid and Newtonian fluid, Dawar et al. [27] explored MHD flow of Maxwell fluid via a velocity slippery stretching sheet with Brownian motion, and thermophoresis. They discovered that an improved temperature field is noticed for increasing the function of the pedesis motion parameter. Kumar et al. [28] investigated magnetite fluid containing nanoparticles through a rotating disk using Noumerov's discretization, considering the accuracy of the finite difference procedure. They reported that at the rotating disk surface, pedesis motion and the Ludwig–Soret effect enhanced the temperature profile while the rate of heat transfer experienced a decline with upsurge values of pedesis motion and the Ludwig–Soret effect. Using the finite element method, Ali et al. [29] investigated hyperbolic tangent Carreau nanofluid via a stretching wedge with pedesis motion and the Ludwig–Soret effect. The rate of heat transport dwindles against the growing values of pedesis motion and the Ludwig–Soret effect. Abbas et al. [30] explored entropy generation on a viscous nanofluid through a horizontal Riga plate. They found that the Brownian motion parameter and thermophoresis parameter improve the energy distribution and its boundary layer thickness. Additionally, the thermophoresis parameter and Brownian motion parameter displayed alternate behavior on nanoparticle concentration distribution. Using the classical Runge–Kutta method, Jayaprakash et al. [31] examined the stagnation point flow of ferromagnetic Oldroyd-B nanofluid via a stretching sheet with Brownian motion and thermophoretic properties. They concluded that increasing the Brownian motion character decreases mass transport with reverse implication of the thermophoretic factor. Shah et al. [32] discussed the suspended nanoparticles in Maxwell fluid in other to enhance thermal transport of the fluid. They revealed that thermal conductivity of the nanofluid improves due to a rise in Brownian motion factor. The increase in the boundary layer thickness is traceable to an upsurge in pedesis motion and the Ludwig–Soret effect. Zeeshan et al. [33] examined the effect of Brownian motion in a nanofluid of a stretchable inclined rotating surface. Some useful research works in this regard are due to Refs. [34–42].

With the exposition of the previous published work, numerous studies on nanofluidic flows have been conducted in a variety of circumstances. However, it is factual to report that little is known about the influence of time dependent radiative nanofluid transport over a bi-directional stretching device with thermal/mass convection taking into consideration the relevance of pedesis motion and Ludwig–Soret flow attributes featuring MHD and heat sink/source. Using the Keller-box method, the objective of this research work is to address some unresolved questions:

i.   What is the comparative effect of the unsteady parameter when it is considered on the bidirectional component of *x*- axis and *y*-axis and when it is not considered?
ii.   How does the presence of magnetic field and absence of it affect the velocity components?
iii.   Whether present or absent, does the stretching parameter have any noticeable influence on f' and g' directions?
iv.   What is the effect of friction coefficients, Nusselt number, and Sherwood number on the model?

2. Mathematical Modeling

The mathematical modeling of the model is completed by adopting the following steps.

2.1. Transport Equations

Bidirectional unsteady stream of incompressible nanofluidic transport on a stretchable device placed in the plane (i.e., $z = 0$). Mechanically, the device is extending in both locations with velocity $u_w(x,t) = \frac{ax}{1-et}$ along $x-$ direction and velocity $v_w(y,t) = \frac{by}{1-et}$ is applied towards $y-$ direction. Here, extending rates are designated by $a > 0$ and $b \geq 0$ along respective directions with dimension [time]$^{-1}$. The unsteadiness of the stretching device is estimated by the constant e with dimension [time]$^{-1}$ satisfying $et < 1$ to create a balance with extending rates. A non-uniform magnetic field with strength $B(t) = \frac{B_0}{\sqrt{1-et}}$ is applied vertically upwards. Inductive effects are negligible by considering the magnetic Reynolds number so small. The modified Buongiorno nanofluid model is adopted to manipulate the significance of pedesis motion designated by coefficient D_B and Ludwig–Soret labeled by coefficient D_T of nanoparticles. The nonlinear form of the thermal radiation term is included. Heat source/sink $Q(t) = \frac{Q^*}{1-et}$ is also linked with the thermal setup.

The temperature of the liquid at the surface is designated by $T_f = T_\infty + A\frac{x^r y^s}{1-et}$ and volume fraction of nano-composition on the same device has been nominated by $C_f = C_\infty + B\frac{x^r y^s}{1-et}$ with ambient positions T_∞, C_∞, respectively. Here, A and B are dimensional constants but (r, s) are non-dimensional power indices used to simultaneous control the temperature/volume fraction of nano-composition at the device in $(x, y)-$ plane, respectively. Leading transport equations in the view of the above-mentioned circumstances are listed as follows: ([24,35]).

$$\frac{\partial u}{\partial x} + \frac{\partial v}{\partial y} + \frac{\partial w}{\partial z} = 0, \tag{1}$$

$$\frac{\partial u}{\partial t} + u\frac{\partial u}{\partial x} + v\frac{\partial u}{\partial y} + w\frac{\partial u}{\partial z} = \vartheta_f \frac{\partial^2 u}{\partial z^2} - \frac{\sigma_f B^2}{\rho_f} u, \tag{2}$$

$$\frac{\partial v}{\partial t} + u\frac{\partial v}{\partial x} + v\frac{\partial v}{\partial y} + w\frac{\partial v}{\partial z} = \vartheta_f \frac{\partial^2 v}{\partial z^2} - \frac{\sigma_f B^2}{\rho_f} v, \tag{3}$$

$$\frac{\partial T}{\partial t} + u\frac{\partial T}{\partial x} + v\frac{\partial T}{\partial y} + w\frac{\partial T}{\partial z} = \alpha_f \frac{\partial^2 T}{\partial z^2} + \tau\left[\frac{D_B}{\Delta C}\frac{\partial C}{\partial z}\frac{\partial T}{\partial z} + \frac{D_T}{T_\infty}\left(\frac{\partial T}{\partial z}\right)^2\right] + \frac{Q}{(\rho C_p)_f}(T - T_\infty) - \frac{1}{(\rho C_p)_f}\frac{\partial q_r}{\partial z}, \tag{4}$$

$$\frac{\partial C}{\partial t} + u\frac{\partial C}{\partial x} + v\frac{\partial C}{\partial y} + w\frac{\partial C}{\partial z} = D_B\frac{\partial^2 C}{\partial z^2} + \frac{D_T \Delta C}{T_\infty}\frac{\partial^2 T}{\partial z^2}. \tag{5}$$

In Equation (4), Q is termed as the heat coefficient used for thermal-absorption or thermal-generation rendering to $Q < 0$ or $Q > 0$, respectively. Further, the factor q_r recognizes the heat flux at the surface in the form of radiation. The Rosseland approximation for a sufficiently thick optical medium is mentioned as follows: ([1,3,6])

$$q_r = -\frac{4}{3K^*} grad(e_b). \tag{6}$$

Here, $e_b = \sigma^* T^4$ offers the Stephan–Boltzmann expression and K^* is included to represent the mean-absorption coefficient. The expression for the non-linear radiation phenomenon is as follows:

$$q_r = -\frac{4\sigma^*}{3K^*}\frac{\partial T^4}{\partial z} = --\frac{16\sigma^*}{3K^*}T^3\frac{\partial T}{\partial z}. \tag{7}$$

2.2. Geometry

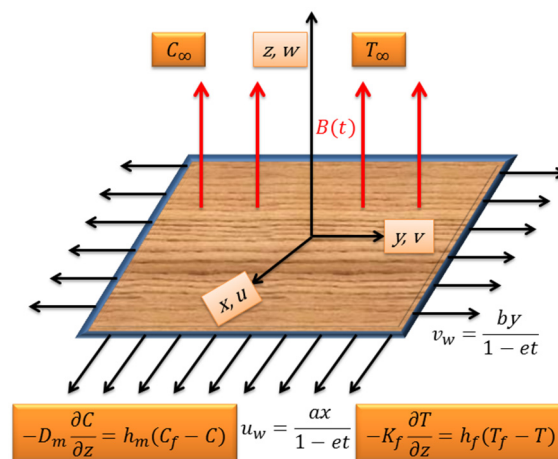The graphical abstract of the present formulation is provided below via Figure 1.

Figure 1. Physical Model of the present model.

2.3. Boundary Restrictions

The related boundary restrictions for the above-mentioned flow with thermal/mass convection are as follows:

$$
\begin{aligned}
at\ z = 0:\ u = \tfrac{ax}{1-et},\ v = \tfrac{by}{1-et}, w = 0, -K_f\tfrac{\partial T}{\partial z} = h_f\left(T_f - T\right), -D_m\tfrac{\partial C}{\partial z} = h_m\left(C_f - C\right) \\
as\ z \to \infty:\ u \to 0, v \to 0, T \to T_\infty, C \to C_\infty
\end{aligned}
\Biggr\}. \tag{8}
$$

Here, D_m offers the molecular-diffusivity of the tiny-sized particle's density, h_f designates the coefficient of wall heat transference, h_m identifies the coefficient of wall mass transference, and K_f represents the thermal conductivity.

2.4. Transformations

It is very necessary to introduce the following transformations to convert the dimensional governing structure placed in Equations (1)–(5) and (8) into the non-dimensional structure before the solution of the problem. These transformations are as follows: ([15,25])

$$
\begin{aligned}
u = \tfrac{ax}{1-et}f'(\zeta), v = \tfrac{ay}{1-et}g'(\zeta), w = -\sqrt{\tfrac{a\vartheta_f}{1-et}}[f(\zeta) + g(\zeta)], \\
\theta(\zeta) = \tfrac{T-T_\infty}{T_f - T_\infty}, \phi(\zeta) = \tfrac{C-C_\infty}{C_f-C_\infty}, \zeta = \sqrt{\tfrac{a}{\vartheta_f(1-et)}}z
\end{aligned}
\Biggr\}. \tag{9}
$$

2.5. Transformed Transport Equations

The transport Equations (2)–(5) have been transformed as mentioned below:

$$
f''' + (f + g)f'' - (f')^2 - \Lambda\left(f' + \tfrac{\zeta}{2}f''\right) - Mf' = 0, \tag{10}
$$

$$
g''' + (f + g)g'' - (g')^2 - \Lambda\left(g' + \tfrac{\zeta}{2}g''\right) - Mg' = 0, \tag{11}
$$

$$
\begin{aligned}
&\tfrac{1}{Pr}(1 + R_d)\theta'' + \tfrac{R_d}{Pr}\Big[(\Gamma - 1)^3\big\{\theta^3\theta'' + 3\theta^2(\theta')^2\big\} + 3(\Gamma - 1)^2\big\{\theta^2\theta'' + 2\theta(\theta')^2\big\} + 3(\Gamma - 1)\big\{\theta\theta'' + (\theta')^2\big\}\Big] \\
&+ (f + g)\theta' - (rf' + sg')\theta - \Lambda\left(\theta + \tfrac{\zeta}{2}\theta'\right) + N_b\theta'\phi' + N_t(\theta')^2 + H_g\theta = 0,
\end{aligned} \tag{12}
$$

$$
\phi'' + \tfrac{N_t}{N_b}\theta'' + Sc\left[(f + g)\phi' - (rf' + sg')\phi - \Lambda\left(\phi + \tfrac{\zeta}{2}\phi'\right)\right] = 0. \tag{13}
$$

2.6. Restructured Boundary Conditions

By adopting the similar procedure, the previous conditions described in Equation (8) are restructured to the format as follows:

$$
\left.
\begin{aligned}
& at\ \zeta = 0 : f'(0) = 1, g'(0) = \alpha, f(0) + g(0) = 0, \\
& \quad \theta'(0) = -Bi_T(1 - \theta(0)), \phi'(0) = -Bi_C(1 - \phi(0)), \\
& as\ \zeta \to \infty : f'(\infty) \to 0, g'(\infty) \to 0, \theta(\infty) \to 0, \phi(\infty) \to 0
\end{aligned}
\right\}
\tag{14}
$$

2.7. Physical Quantities

In the micro and nano level study, the estimation of physical quantities is key to inspecting the technological and engineering aspects of the flow. According to the present modeling, drag forces along both sides/directions, Nusselt number (i.e., rate of heat transfer), and the Sherwood number (i.e., rate of mass transfer) are demarcated as:

$$
Cf_x = \frac{\tau_{zx}}{\frac{1}{2}\rho_f u_w{}^2}, \text{ with} \tau_{zx} = \mu_f \left(\frac{\partial u}{\partial z} \right)_{z=0},
\tag{15}
$$

$$
Cf_y = \frac{\tau_{zy}}{\frac{1}{2}\rho_f v_w{}^2}, \text{ with} \tau_{zy} = \mu_f \left(\frac{\partial v}{\partial z} \right)_{z=0},
\tag{16}
$$

$$
Nu_x = \frac{x q_w}{K_f \left(T_f - T_\infty \right)}, \text{ with} q_w = -K_f \left(\frac{\partial T}{\partial z} \right)_{z=0} + (q_r)_{z=0},
\tag{17}
$$

$$
Sh_x = \frac{x q_m}{D_B \left(C_f - C_\infty \right)}, \text{ with } q_m = -D_B \left(\frac{\partial C}{\partial z} \right)_{z=0}.
\tag{18}
$$

The non-dimensional form of Equations (15)–(18) are as follows:

$$
Cf_{rx} = Re_x^{\frac{1}{2}} C_{fx} = 2f''(0),
\tag{19}
$$

$$
Cf_{ry} = Re_y^{\frac{1}{2}} C_{fy} = 2g''(0),
\tag{20}
$$

$$
Nu_r = Re_x^{-\frac{1}{2}} Nu_x = -\left[1 + R_d \{ 1 + \theta(0)(\Gamma - 1) \}^3 \right] \theta'(0),
\tag{21}
$$

$$
Sh_r = Re_x^{-\frac{1}{2}} Sh_x = -\phi'(0).
\tag{22}
$$

2.8. Dimensionless Numbers/Parameters

The dimensionless numbers and parameters involved in the present modeling are unsteady parameter $\left(\Lambda = \frac{e}{a} \right)$, Hartmann number $\left(M = \frac{\sigma B_0{}^2}{\rho_f a} \right)$, Prandtl number $\left(Pr = \frac{\vartheta_f}{\alpha_f} \right)$, radiation parameter $\left(R_d = \frac{4\sigma^* T_\infty{}^3}{3K^* K_f} \right)$, temperature-ratio parameter $\left(\Gamma = \frac{T_f}{T_\infty} \right)$, pedesis motion parameter $\left(N_b = \frac{\tau D_B (C_f - C_\infty)}{\Delta C \vartheta_f} \right)$, Ludwig–Soret parameter $\left(N_t = \frac{\tau D_T (T_f - T_\infty)}{\vartheta_f T_\infty} \right)$, heat consumption/production parameter $\left(H_g = \frac{Q^*}{a (\rho C_p)_f} \right)$, Schmidt number $\left(Sc = \frac{\vartheta_f}{D_B} \right)$, bi-directional stretching-ratio parameter $\left(\alpha = \frac{b}{a} \right)$, thermal Biot number $\left(Bi_T = \frac{h_f}{K_f} \sqrt{\frac{\vartheta_f}{a}} \right)$, concentration Biot number $\left(Bi_C = \frac{h_m}{D_m} \sqrt{\frac{\vartheta_f}{a}} \right)$, local Reynold's number corresponding to $x-$ axis $\left(Re_x = \frac{x u_w}{\vartheta_f} \right)$, and local Reynold's number corresponding to $y-$ axis $\left(Re_y = \left(\frac{b}{a} \right)^3 \frac{y v_w}{\vartheta_f} \right)$.

3. Numerical Simulation

3.1. Keller-Box Method Procedure

The restructured transport equations have been solved through implicit finite difference-based mechanisms termed the Keller-box method. Keeping the procedure of this method in mind, higher order ODEs (10)–(13) are reorganized into first-order ODEs and boundary conditions (14) are adjusted according to new/fresh variables as follows:

$$
\begin{pmatrix} f' \\ f'' \\ f''' \\ g' \\ g'' \\ g''' \\ \theta' \\ \theta'' \\ \phi' \\ \phi'' \end{pmatrix} = \begin{pmatrix} f_1 \\ f_2 \\ f_2' \\ g_1 \\ g_2 \\ g_2' \\ \theta_1 \\ \theta_1' \\ \phi_1 \\ \phi_1' \end{pmatrix} = \begin{pmatrix} f_1 \\ f_2 \\ -(f+g)f_2 + (f_1)^2 + \Lambda\left(f_1 + \frac{\zeta}{2}f_2\right) + Mf_1 \\ g_1 \\ g_2 \\ -(f+g)g_2 + (g_1)^2 + \Lambda\left(g_1 + \frac{\zeta}{2}g_2\right) + Mg_1 \\ \theta_1 \\ \frac{-R_d\left[3(\Gamma-1)^3\theta^2(\theta_1)^2+6(\Gamma-1)^2\theta(\theta_1)^2+3(\Gamma-1)(\theta_1)^2\right]}{(1+R_d+R_d[(\Gamma-1)^3\theta^3+3(\Gamma-1)^2\theta^2+3(\Gamma-1)\theta])} - \\ \frac{Pr\left[(f+g)\theta_1-(rf_1+sg_1)\theta-\Lambda\left(\theta+\frac{\zeta}{2}\theta_1\right)+N_b\theta_1\phi_1+N_t(\theta_1)^2+H_g\theta\right]}{(1+R_d+R_d[(\Gamma-1)^3\theta^3+3(\Gamma-1)^2\theta^2+3(\Gamma-1)\theta])} \\ \phi_1 \\ -\frac{N_t}{N_b}\theta_2 - Sc\left[(f+g)\phi_1 - (rf_1+sg_1)\phi - \Lambda\left(\phi+\frac{\zeta}{2}\phi_1\right)\right] \end{pmatrix}, \quad (23)
$$

with the BCs

$$
\begin{pmatrix} f(0) \\ f_1(0) \\ f_1(6) \\ g(0) \\ g_1(0) \\ g_1(6) \\ \theta_1(0) \\ \theta(6) \\ \phi_1(0) \\ \phi_1(6) \end{pmatrix} = \begin{pmatrix} 0 \\ 1 \\ 0 \\ 0 \\ \alpha \\ 0 \\ -Bi_T(1-\theta(0)) \\ 0 \\ -Bi_C(1-\phi(0)) \\ 0 \end{pmatrix}. \quad (24)
$$

Equations (23) and (24) are then transformed into difference equations by incorporating central difference and average center approximations before the implementation of Newton's iterative formula. A linearized tri-diagonal system is formed by the omission of quadratic and higher order terms in the change of the variable. Finally, the tri-diagonal block matrices system is solved via the LU-decomposition technique.

3.2. Solution Convergence

The grid independence approach is used for convergence analysis. Initially, less numbers of grid points with step size $\Delta\zeta = 1/5$ are opted to start the convergence analysis with the far field boundary effect, say $\zeta_\infty = 20$ and then numbers of grid points are increased to achieve the convergence of the solution with desired accuracy, i.e., up to the fifth decimal place. The results are displayed in Table 1.

3.3. Code Validation

The assurance of the current scrutiny in association with previous published reports is accessed in this section. Here, we have computed the outputs of $f''(0)$, $g''(0)$, $f(\infty)$, $g(\infty)$ for diverse choices of α and then obtained outcomes have been compared with the published reports of Wang [42] and Liu and Andersson [41]. The outputs are reflected in Table 2 and an excellent scientific connection has been revealed with previous reports.

Table 1. Convergence analysis with $Pr = 6.2$, $\alpha = 0.3$, $Sc = 0.4$, $r = 1.0$, $s = 2.0$, $\Lambda = 0.6$, $M = 0.7$, $R_d = 0.8$, $\Gamma = 1.4$, $H_g = 0.2$, $Bi_T = 0.5$, $Bi_C = 0.3$, $N_t = 0.4$, $N_b = 0.5$.

Grid Points	Step Size	$-f''(0)$	$-g''(0)$	$-\theta'(0)$	$-\phi'(0)$
100	1/5	1.49809	0.39968	0.4051	0.14813
500	1/25	1.49852	0.39959	0.40504	0.14822
1000	1/50	1.49854	0.39958	0.40503	0.14822
1500	1/75	1.49854	0.39958	0.40503	0.14822

Table 2. Scientific connection with previous reports via numerical comparison.

$\alpha = 1.0$	$f(\infty)$	$g(\infty)$	$-f''(0)$	$-g''(0)$
Present scrutiny	0.751498	0.751498	1.173722	1.173722
Liu and Andersson [41]	0.751494	0.751494	1.173721	1.173721
Wang [42]	0.751527	0.751527	1.173720	1.173720
$\alpha = 0.5$	$f(\infty)$	$g(\infty)$	$-f''(0)$	$-g''(0)$
Present scrutiny	0.842387	0.451678	1.093095	0.465205
Liu and Andersson [41]	0.842360	0.451663	1.093096	0.465206
Wang [42]	0.842360	0.451671	1.093097	0.465205
$\alpha = 0.0$	$f(\infty)$	$g(\infty)$	$-f''(0)$	$-g''(0)$
Present scrutiny	1.0	0.0	−1.0	0.0
Liu and Andersson [41]	1.0	0.0	−1.0	0.0
Wang [42]	1.0	0.0	−1.0	0.0

4. Results and Discussion

The implications of available parameters on velocity, temperature, concentration distributions, friction coefficients, Nusselt and Sherwood numbers are investigated in this segment as reported in the generated Figures 2–17 and Tables 3–5.
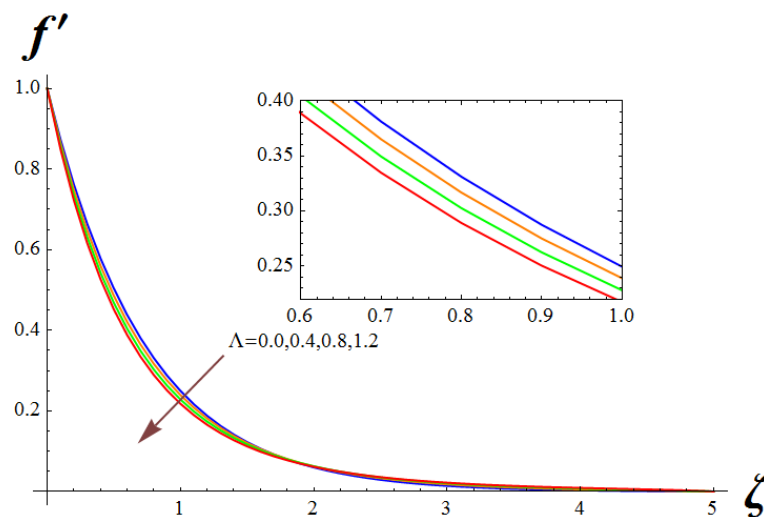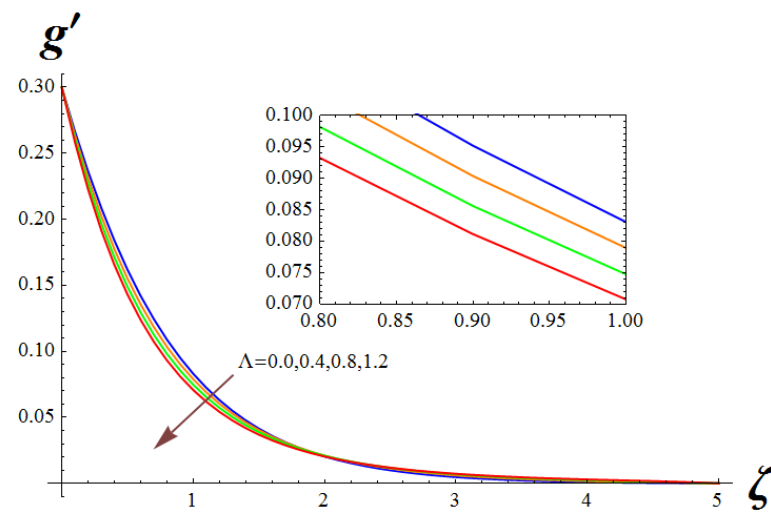

Figure 2. Character of Λ on f'.
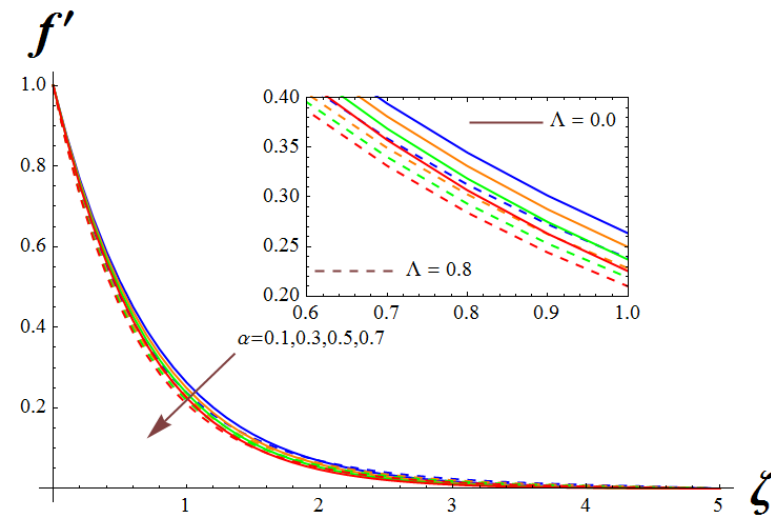
Figure 3. Character of Λ on g'.

Figure 4. Character of α on f'.
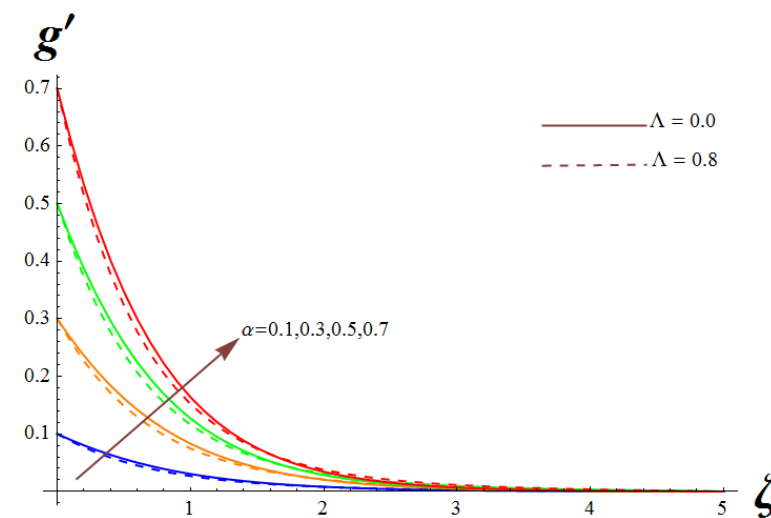
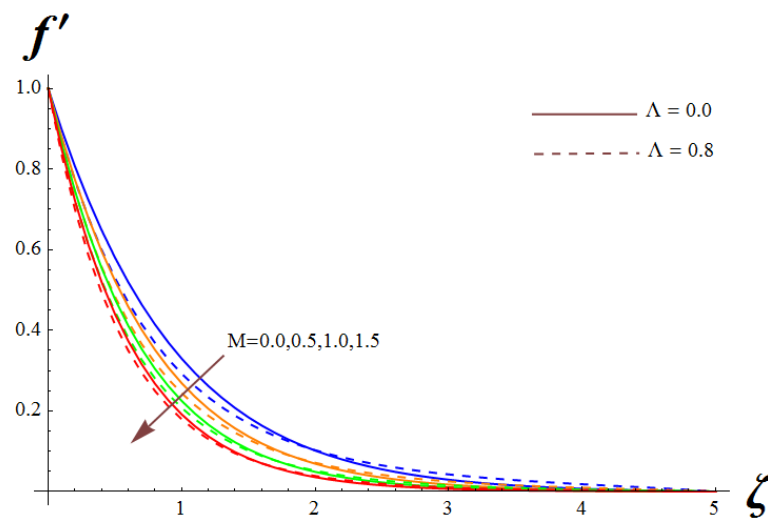**Figure 5.** Character of α on g'.

Figure 6. Character of M on f'.
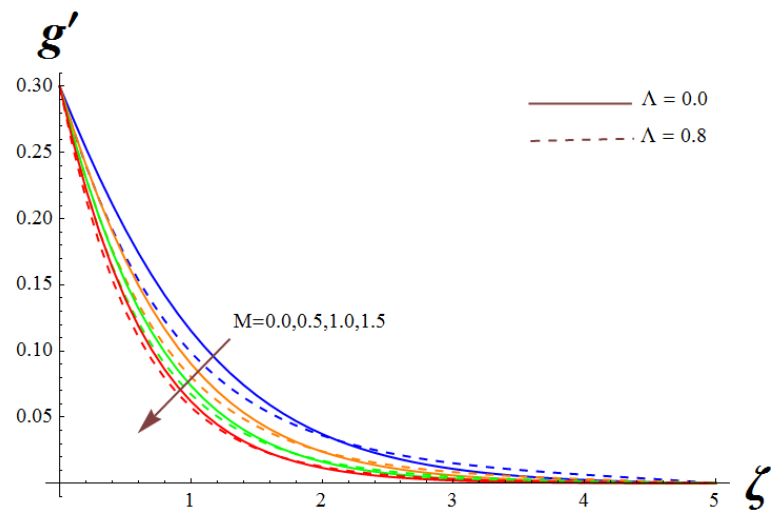
Figure 7. Character of M on g'.
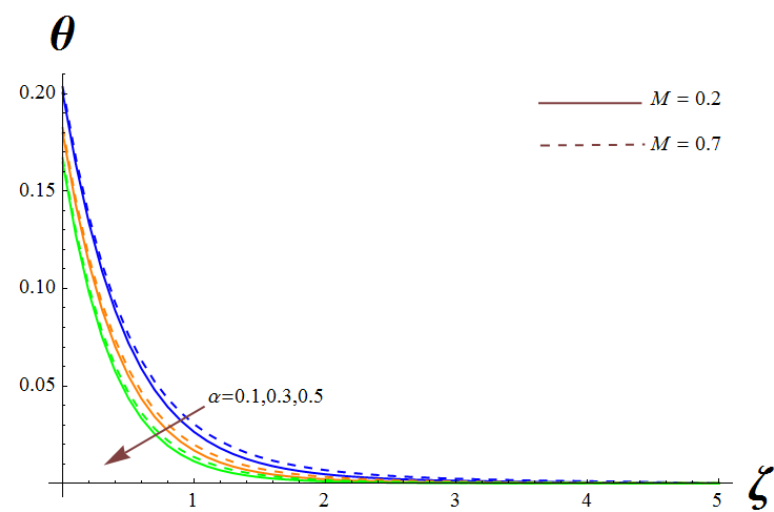
Figure 8. Character of α on θ.
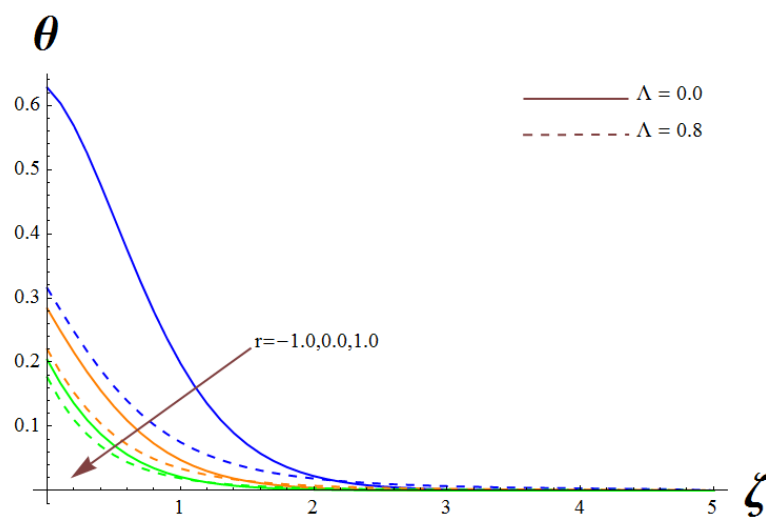
Figure 9. Character of r on θ.
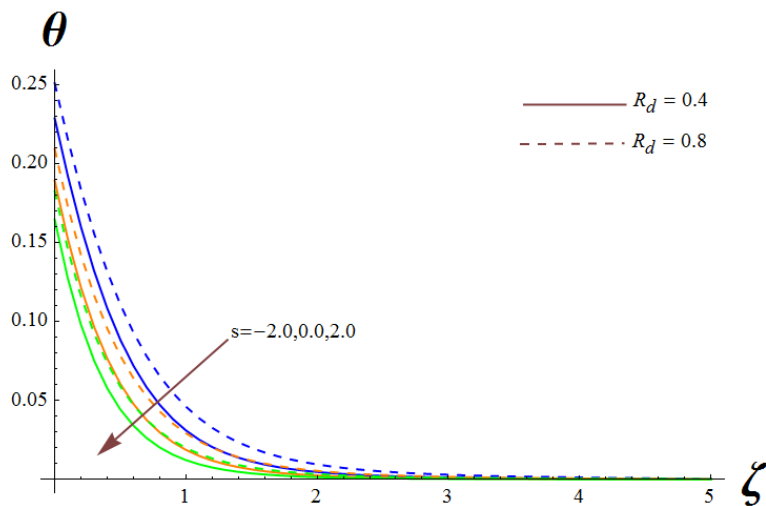
Figure 10. Character of s on θ.
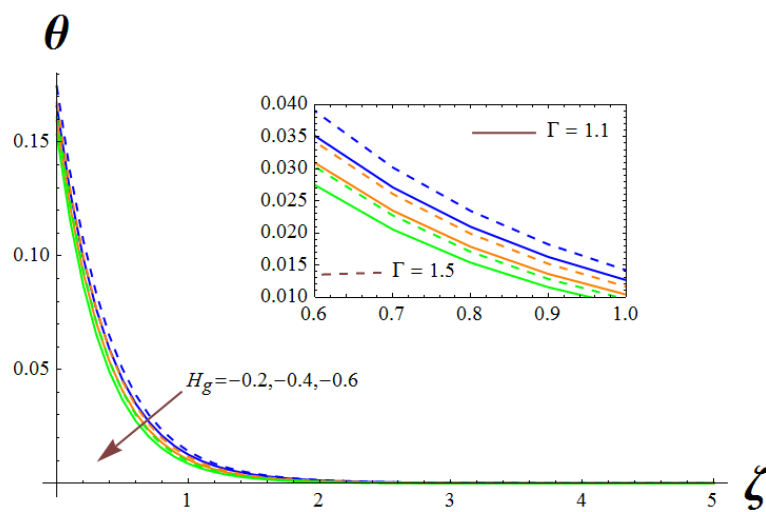
Figure 11. Character of Hg (heat sink) on θ.
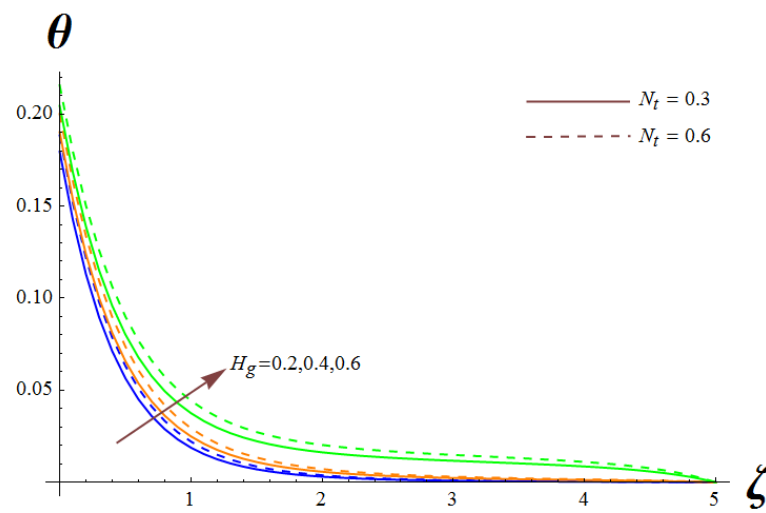
Figure 12. Character of Hg (heat source) on θ.
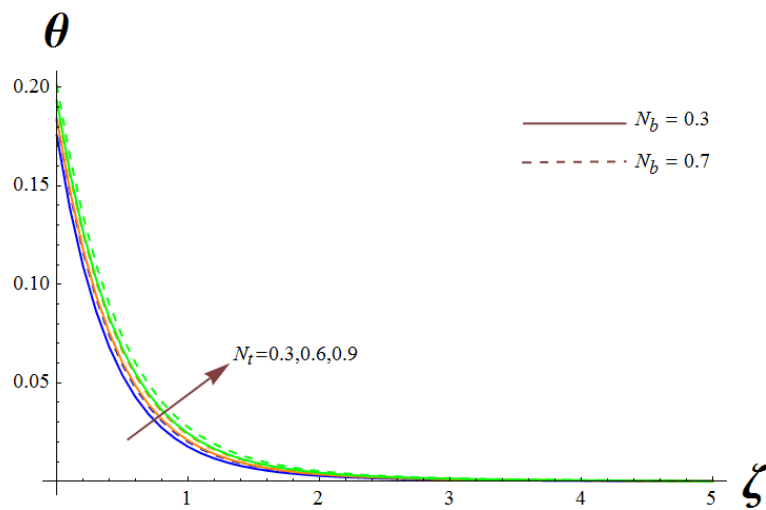
Figure 13. Character of N_t on θ.
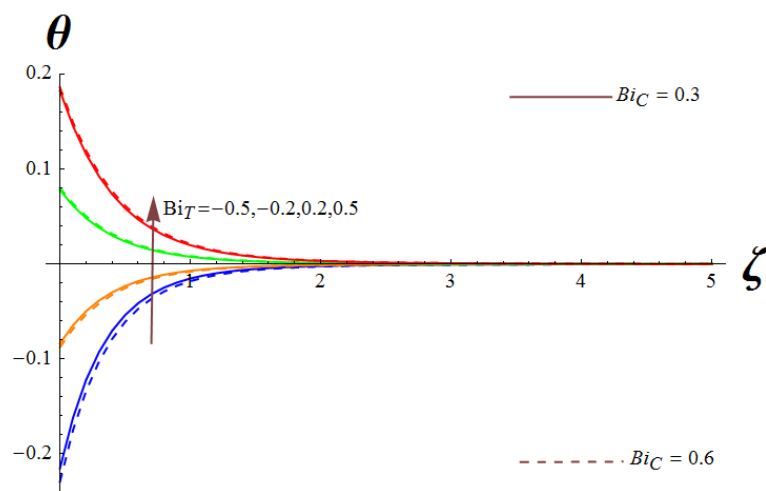
Figure 14. Character of Bi_T on θ.
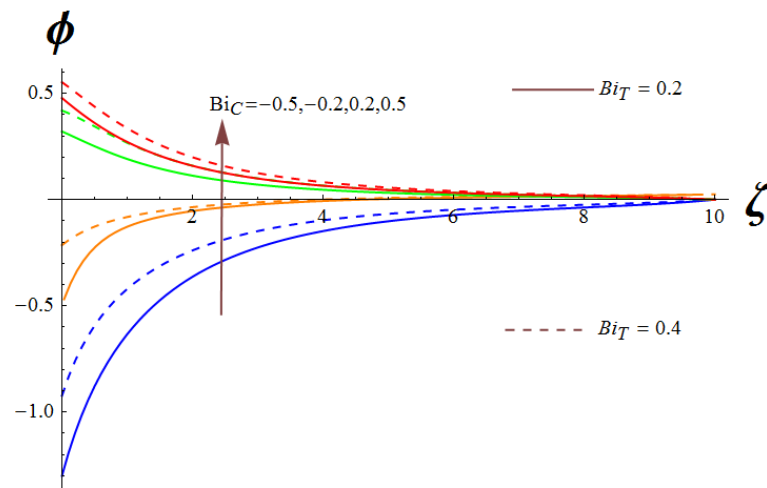
Figure 15. Character of Bi_C on ϕ.
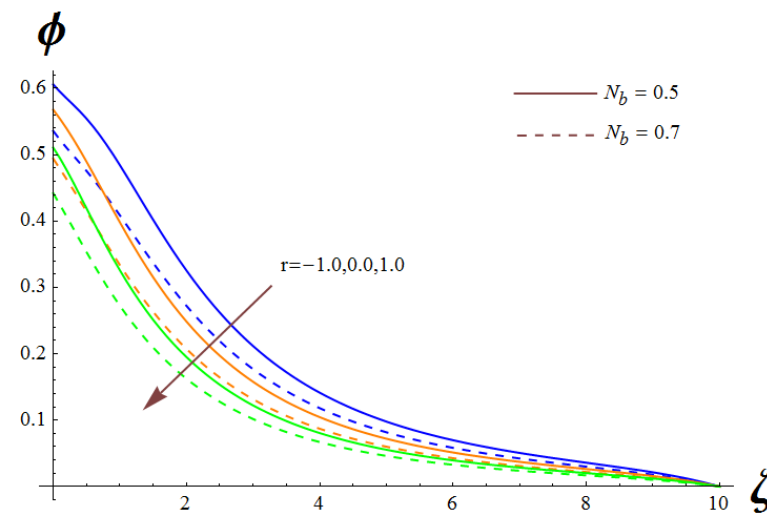
Figure 16. Character of r on ϕ.
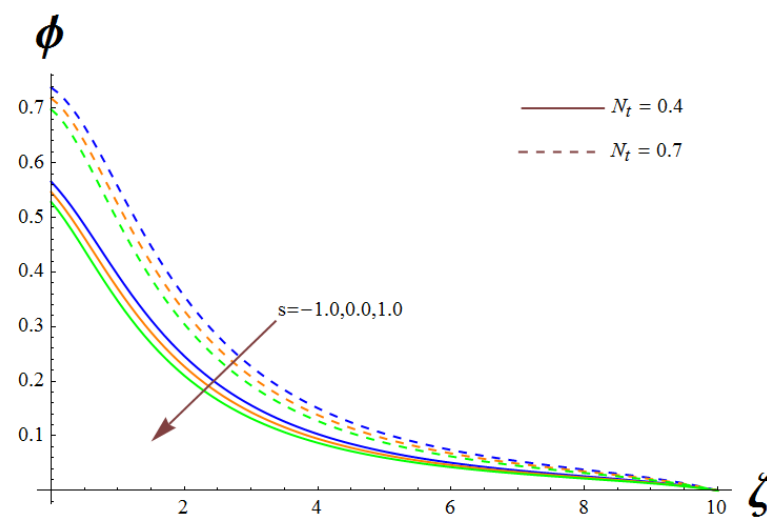
Figure 17. Character of s on ϕ.

Table 3. Skin-friction analysis Cf_{rx} and Cf_{ry} for dissimilar values of α, M, and Λ.

α	M	Λ	Cf_{rx}	Cf_{ry}
0.1	0.5	0.4	−2.703724	−0.221048
0.5			−2.805763	−1.277634
0.9			−2.903119	−2.57092
0.2	0.3		−2.578544	−0.423887
	0.6		−2.802237	−0.477544
	0.9		−3.009137	−0.525623
	0.4	0.2	−2.543627	−0.416068
		0.6	−2.764274	−0.468131
		0.9	−2.922576	−0.504867

Table 4. Heat transfer analysis Nu_r for dissimilar values of Bi_T, Λ, H_g, and Γ.

Bi_T	Λ	H_g	Γ	Nu_r
0.3	0.5	0.2	1.1	0.480382
0.5				0.741029
0.7				0.962075
0.9	0.4			1.14159
	0.8			1.17459
	1.2			1.202528
	1.6	0.4		1.210284
		0.6		1.192313
		0.8		1.171314
		1.1	1.3	1.209605
			1.5	1.374133
			1.7	1.548237

Table 5. Mass transfer analysis Sh_r for dissimilar values of Bi_C, Λ, N_b, and N_t.

Bi_C	Λ	N_b	N_t	Sh_r
0.3	0.5	0.2	0.3	0.069379
0.5				0.096893
0.7				0.11673
0.9	0.4			0.11797
	0.8			0.16536
	1.2			0.1995
	1.6	0.3		0.306
		0.4		0.34569
		0.5		0.36951
		0.6	0.4	0.36094
			0.5	0.33677
			0.6	0.3129

In graphical numbering, Figures 2 and 3 show that the horizontal velocity aspect of both the *x*- and *y*-axis pathway of the nanofluidic transport features is a declining

attribute of the unsteady parameter (Λ = e/a) within the range of $0.0 \leq \Lambda \leq 1.2$. Due to the relationship between a and Λ, the augmentation of a in its positive sense of values boost Λ, which implies an incremental stretching rate. Consequently, the velocity of the nanofluid declines given the augmentation values of Λ. Furthermore, a decline is noticed for friction coefficients on both the x- and y-axis pathway as revealed in Table 3. Figure 4 presents the effect of the stretching parameter (α) on f' in the presence of the unsteady parameter (Λ) and in the absence of the unsteady parameter (Λ). The growing values of the stretching parameter (α) decreases f', with greater downfall in the presence of the unsteady parameter (Λ) than in the absence of the unsteady parameter (Λ). Given that (α = b/a), augmenting the values of the stretching parameter (α) connotes that the stretching ratio (a) along the x-axis diminishes, which results in decline of f'. Moreso, as reported in Table 3, the friction coefficient in the x-axis experiences a decline as the values of the stretching parameter increases. Figure 5 shows the effect of the stretching parameter (α) on g'. The growing values of the stretching parameter (α) increases g', with a greater upshot in the absence of the unsteady parameter (Λ) than in the presence of the unsteady parameter (Λ), which is expected from the mathematical relationship (α = b/a). Conversely, the friction coefficient in the y-axis drops as the values of the stretching parameter increases. The magnetic field (M) parameter range $0.0 \leq M \leq 2.0$ in Figures 6 and 7 establishes that the velocity component of both x- and y-direction nanofluidic transport processes diminishes with increased magnetic field values, with a concurrent greater downfall in the presence of the unsteady parameter (Λ) than in the absence of the unsteady parameter (Λ). The downfall of the velocity component is traceable to the Lorentzian force created by the augmentation of the magnetic field values. In addition, a downfall is reported for friction coefficients on both the x- and y-axis pathway as revealed in Table 3. Figure 8 demonstrates the influence of the stretching parameter ($0.1 \leq \alpha \leq 1.0$) on temperature profiles, taking into cognizance the increasing values of M. The effect of the stretching parameter shows a decline in the nanofluid temperature gradient. In Figure 9, the power index r shows a decreasing impact on nanofluid temperature distribution in the presence of the unsteady parameter (Λ) and in the absence of the unsteady parameter (Λ). Similarly, In Figure 10, the power index s shows a decreasing impact on nanofluid temperature distribution in the presence of an incremental impact of thermal radiation. With distinct values of the temperature-ratio parameter as shown in Figure 11, thermal-absorption parameter values are found to decrease nanofluid temperature distribution. More so, in Tables 4 and 5, the rate of heat transfer and mass transfer improves with an upshot in the temperature-ratio parameter. As expected, the thermal source parameter enhances nanofluid temperature distribution, as seen in Figure 12, in the presence of an increasing Ludwig–Soret parameter. On the contrary, the rate of heat transaction (Nu_r) drops with enhanced values of heat generation. In Figure 13, the Ludwig–Soret parameter empowers nanofluid temperature distribution in the presence of an increasing pedesis motion parameter. Figure 14 shows the improvement of nanofluid temperature distribution as the values of the Biot number Bi_T increase. Similarly, the rate of heat transfer rises when Bi_T increases as displayed in Table 4. In Figure 15, concentration distribution is enhanced as the concentration Boit number Bi_C increases, with a corresponding effect on mass transfer. In Figure 16, the power index r shows a decreasing impact on concentration distribution in the presence of an increasing pedesis motion parameter. Similarly, in Figure 17, the power index s shows a decreasing impact on concentration distribution in the presence of an incremental impact of the Ludwig–Soret parameter.

5. Conclusions

In this report, the nonlinear radiative nanofluidic hydrothermal unsteady bidirectional transport with thermal/mass convection aspect has been investigated using the Keller-box method. Based on the analysis of the results, it is worth concluding that:

- The decline in the velocity components of the x-axis and y-axis direction is due to progressive flourishing of the unsteady parameter and magnetic field.

- Temperature distribution rises with a corresponding increase in the values of the heat source, Ludwig–Soret factor, temperature Biot number with an opposite effect for heat sink, stretching parameter, and power indices of r and s.
- Given the growth of the concentration Biot number, power indices of r and s, the concentration of the nanofluidic is enhanced.
- Friction coefficients decline for the stretching parameter, magnetic field, and unsteady parameter growth along the bidirectional velocity components.
- The rate of heat transmission is amplified with the temperature ratio and temperature Biot number and a reverse effect is noticed for the heat source and unsteady parameter.
- Mass transfer is enhanced for pedesis motion, unsteady parameter, and the concentration Biot number, with reverse impact of the Ludwig–Soret parameter.

In the future, this work can be extended for non-Newtonian nanofluids, hybrid-nanofluids, tri-hybrid nanofluids, and ternary hybrid nanofluids.

References

1. Seddeek, M.A. Effects of radiation and variable viscosity on a MHD free convection flow past a semi-infinite flat plate with an aligned magnetic field in the case of unsteady flow. *Int. J. Heat Mass Transf.* **2001**, *45*, 931–935. [CrossRef]
2. Mushtaq, A.; Mustafa, M.; Hayat, T.; Alsaedi, A. Nonlinear radiative heat transfer in the flow of nanofluid due to solar energy: A numerical study. *J. Taiwan Inst. Chem. Eng.* **2014**, *45*, 1176–1183. [CrossRef]
3. Lu, D.; Ramzan, M.; Ahmad, S.; Shafee, A.; Suleman, M. Impact of Nonlinear Thermal Radiation and Entropy Optimization Coatings with Hybrid Nanoliquid Flow Past a Curved Stretched Surface. *Coatings* **2018**, *8*, 430. [CrossRef]
4. Mahanthesh, B.; Thriveni, K. Significance of inclined magnetic field on nano-bioconvection with nonlinear thermal radiation and exponential space based heat source: A sensitivity analysis. *Eur. Phys. J. Spec. Top.* **2021**, *230*, 1487–1501. [CrossRef]
5. Rana, P.; Dhanai, R.; Kumar, L. Radiative nanofluid flow and heat transfer over a non-linear permeable sheet with slip conditions and variable magnetic field: Dual solutions. *Ain Shams Eng. J.* **2017**, *8*, 341–352. [CrossRef]
6. Bhatti, M.M.; Abbas, T.; Rashidi, M.M. Numerical study of entropy generation with nonlinear thermal radiation on Magnetohydrodynamics non-Newtonian nanofluid through a porous shrinking sheet's. *Magnetics* **2016**, *21*, 468–475. [CrossRef]
7. Ashraf, A.W.; Alghtani, A.H.; Khan, I.; Andualem, M. Thermal Transport in Radiative Nanofluids by Considering the Influence of Convective Heat Condition. *J. Nanomater.* **2022**, *2022*, 1854381.
8. Mustafa, M.; Mushtaq, A.; Hayat, T.; Ahmad, B. Nonlinear Radiation Heat Transfer Effects in the Natural Convective Boundary Layer Flow of Nanofluid Past a Vertical Plate: A Numerical Study. *PLoS ONE* **2014**, *9*, e103946. [CrossRef]
9. Imran, M.; Farooq, U.; Muhammad, T.; Khan, S.U.; Waqas, H. Bioconvection transport of Carreau nanofluid with magnetic dipole and nonlinear thermal radiation. *Case Stud. Therm. Eng.* **2021**, *26*, 101129. [CrossRef]
10. Khan, U.; Ahmed, N.; Mohyud-Din, S.T.; Bin-Mohsin, B. Nonlinear radiation effects on MHD flow of nanofluid over a nonlinearly stretching/shrinking wedge. *Neural Comput. Appl.* **2017**, *28*, 2041–2050. [CrossRef]
11. Ramzan, M.; Yousaf, F. Boundary layer flow of three-dimensional viscoelastic nanofluid past a bi-directional stretching sheet with Newtonian heating. *AIP Adv.* **2015**, *5*, 057132. [CrossRef]
12. Hayat, T.; Muhammad, T.; Shehzad, S.A.; Alsaedi, A. Similarity solution to three dimensional boundary layer flow of second grade nanofluid past a stretching surface with thermal radiation and heat source/sink. *AIP Adv.* **2015**, *5*, 017107. [CrossRef]
13. Javed, T.; Faisal, M.; Ahmad, I. Actions of viscous dissipation and Ohmic heating on bidirectional flow of a magneto-Prandtl nanofluid with prescribed heat and mass fluxes. *Heat Transf.* **2020**, *49*, 4801–4819. [CrossRef]

14. Ahmad, I.; Faisal, M.; Zan-Ul-Abadin, Q.; Javed, T.; Loganathan, K. Unsteady 3D heat transport in hybrid nanofluid containing brick shaped ceria and zinc-oxide nanocomposites with heat source/sink. *Nanocomposites* **2022**, *8*, 1–12. [CrossRef]

15. Khan, S.U.; Alabdan, R.; Al-Qawasmi, A.; Vakkar, A.; Handa, M.B.; Tlili, I. Bioconvection applications for double stratification 3-D flow of Burgers nanofluid over a bidirectional stretched surface: Enhancing energy system performance. *Case Stud. Therm. Eng.* **2021**, *26*, 101073. [CrossRef]

16. Faisal, M.; Ahmad, I.; Javed, T. Significances of prescribed heat sources on magneto Casson nanofluid flow due to unsteady bi-directionally stretchable surface in a porous medium. *SN Appl. Sci.* **2020**, *2*, 1472. [CrossRef]

17. Gupta, S.; Gupta, S. MHD three dimensional flow of Oldroyd-B nanofluid over a bidirectional stretching sheet: DTM-Padé Solution. *Nonlinear Eng.* **2019**, *8*, 744–754. [CrossRef]

18. Bag, R.; Kundu, P.K. Radiative nanofluidic transport over bidirectional stretching sheet with multiple convective conditions and heat source/sink. *Partial. Differ. Equ. Appl. Math.* **2022**, *5*, 100358. [CrossRef]

19. Ahmad, I.; Khurshid, I.; Faisal, M.; Javed, T.; Abbas, Z. Mixed convective flow of an Oldroyd-B nanofluid impinging over an unsteady bidirectional stretching surface with the significances of double stratification and chemical reaction. *SN Appl. Sci.* **2020**, *2*, 1599. [CrossRef]

20. Munir, A.; Shahzad, A.; Khan, M. Convective Flow of Sisko Fluid over a Bidirectional Stretching Surface. *PLoS ONE* **2015**, *10*, e0130342. [CrossRef]

21. Bilal, S.; Rehman, K.U.; Malik, M.Y.; Hussain, A.; Khan, M. Effects of temperature dependent conductivity and absorptive/generative heat transfer on MHD three dimensional flow of Williamson fluid due to bidirectional non-linear stretching surface. *Results Phys.* **2017**, *7*, 204–212. [CrossRef]

22. Raju, C.S.; Sandeep, N. Heat and Mass Transfer in 3D Non-Newtonian Nano and Ferro Fluids over a Bidirectional Stretching Surface. *Int. J. Eng. Res. Afr.* **2015**, *21*, 33–51. [CrossRef]

23. Ahmad, R.; Mustafa, M.; Hayat, T.; Alsaedi, A. Numerical study of MHD nanofluid flow and heat transfer past a bidirectional exponentially stretching sheet. *J. Magn. Magn. Mater.* **2016**, *407*, 69–74. [CrossRef]

24. Ahmad, I.; Faisal, M.; Javed, T. Magneto-nanofluid flow due to bidirectional stretching surface in a porous medium. *Spéc. Top. Rev. Porous Media Int. J.* **2019**, *10*, 457–473. [CrossRef]

25. Ahmad, I.; Faisal, M.; Javed, T. Bi-directional stretched nanofluid flow with Cattaneo–Christov double diffusion. *Results Phys.* **2019**, *15*, 102581. [CrossRef]

26. Afify, A.A. The influence of slip boundary condition on Casson nanofluid flow over a stretching sheet in the presence of viscous dissipation and chemical reaction. *Math. Probl. Eng.* **2017**, *2017*, 3804751. [CrossRef]

27. Dawar, A.; Saeed, A.; Shah, Z.; Kumam, W.; Islam, S.; Kumam, P. Analytical Simulation for Magnetohydrodynamic Maxwell Fluid Flow Past an Exponentially Stretching Surface with First-Order Velocity Slip Condition. *Coatings* **2021**, *11*, 1009. [CrossRef]

28. Kumar, R.; Bhattacharyya, A.; Seth, G.S.; Chamkha, A.J. Transportation of magnetite nanofluid flow and heat transfer over a rotating porous disk with Arrhenius activation energy: Fourth order Noumerov's method. *Chin. J. Phys.* **2021**, *69*, 172–185. [CrossRef]

29. Ali, B.; Naqvi, R.A.; Mariam, A.; Ali, L.; Aldossary, O.M. Finite Element Study for Magnetohydrody namic (MHD) Tangent Hyperbolic Nanofluid Flow over a Faster/Slower Stretching Wedge with Activation Energy. *Mathematics* **2021**, *9*, 25. [CrossRef]

30. Abbas, T.; Ayub, M.; Bhatti, M.M.; Rashidi, M.M.; Ali, M.E. Entropy Generation on Nanofluid Flow through a Horizontal Riga Plate. *Entropy* **2016**, *18*, 223. [CrossRef]

31. Jayaprakash, M.C.; Asogwa, K.K.; Lalitha, K.R.; Veeranna, Y.; Sreenivasa, G.T. Passive control of nanoparticles in stagnation point flow of Oldroyd-B Nanofluid with aspect of magnetic dipole. *Part E J. Process Mech. Eng.* **2021**. [CrossRef]

32. Shah, N.A.; Tosin, O.; Shah, R.; Salah, B.; Chung, J.D. Brownian motion and thermophoretic diffusion effects on the dynamics of MHD upper convected maxwell nanofluid flow past a vertical surface. *Phys. Scr.* **2021**, *96*, 125722. [CrossRef]

33. Zeeshan; Rasheed, H.U.; Khan, W.; Khan, I.; Alshammari, N.; Hamadneh, N. Brownian motion of thin film nanofluid flow of convective heat transfer over a stretchable rotating surface. *Sci. Rep.* **2022**, *12*, 2708. [CrossRef] [PubMed]

34. Shah, Z.; Gul, T.; Islam, S.; Khan, M.A.; Bonyah, E.; Hussain, F.; Mukhtar, S.; Ullah, M. Three dimensional third grade nanofluid flow in a rotating system between parallel plates with brownian motion and thermophoresis effects. *Results Phys.* **2018**, *10*, 36–45. [CrossRef]

35. Rafique, K.; Anwar, M.I.; Misiran, M.; Khan, I.; Alharbi, S.O.; Thounthong, P.; Nisar, K.S. Keller-Box Analysis of Buongiorno Model with Brownian and Thermophoretic Diffusion for Casson Nanofluid over an Inclined Surface. *Symmetry* **2019**, *11*, 1370. [CrossRef]

36. Ali, L.; Islam, S.; Gul, T.; Khan, I.; Dennis, L.C.; Khan, W.; Khan, A. The Brownian and Thermophoretic analysis of the non-newtonian Williamson fluid flow of thin film in a porous space over an unstable stretching surface. *Appl. Sci.* **2017**, *7*, 404. [CrossRef]

37. Islam, Z.; Azad, A.K.; Hasan, M.J.; Hossain, R.; Rahman, M.M. Unsteady periodic natural convection in a triangular enclosure heated sinusoidally from the bottom using CNT-water nanofluid. *Results Eng.* **2022**, *14*, 100376. [CrossRef]

38. Asogwa, K.K.; Mebarek-Oudina, F.; Animasaun, I.L. Comparative investigation of water-based Al_2O_3 Nanoparticles through water-based CuO nanoparticles over an exponentially accelerated radiative Riga plate surface via heat transport. *Arab. J. Sci. Eng.* **2022**, *47*, 8721–8738. [CrossRef]

39. Asogwa, K.K.; Uwanta, I.J.; Momoh, A.A.; Omokhuale, E. Heat and mass transfer over a vertical plate with periodic Suction and heat sink. *Res. J. Appl. Sci. Eng. Technol.* **2013**, *5*, 7–15. [CrossRef]
40. Shoaib, M.; Khan, R.A.; Ullah, H.; Nisar, K.S.; Raja, M.A.Z.; Islam, S.; Felemban, B.F.; Yahia, I.S. Heat transfer impacts on Maxwell nanofluid flow over a vertical moving surface with MHD using stochastic numerical technique via artificial neural networks. *Coatings* **2021**, *11*, 1483. [CrossRef]
41. Liu, I.C.; Andersson, H.I. Heat transfer over a bidirectional stretching sheet with variable thermal conditions. *Int. J. Heat Mass Transf.* **2008**, *51*, 4018–4024. [CrossRef]
42. Wang, C.Y. The three dimensional flow due to a stretching flat surface. *Phys. Fluids* **1984**, *27*, 1915–1917. [CrossRef]